On potential challenges of V2X sidelink relaying under interference: link-level and system-level simulation with neural network assisted

Chonghao Zhao[1] and Gang Wu[1*]

*Correspondence:
wugang99@uestc.edu.cn

[1] National Key Laboratory of Wireless Communications, University of Electronic Science and Technology of China, Chengdu 611731, Sichuan, China

Abstract

The ever-increasing demand for high data rates and high connection densities in the vehicle communication network, along with the widespread adoption of radio access over the Third Generation Partnership Project (3GPP) standard, has been a major driver for the research on cellular vehicle-to-everything (C-V2X) communication. Nevertheless, Wi-Fi and other wireless communication technology work on the 5.9 GHz unlicensed band has also undergone booming proliferation over the years. C-V2X users dedicated band on the 5.9 GHz spectrum may thus suffer from both co-channel and adjacent channel interference, which cannot be negligible, especially in urban scenarios. To this end, 3GPP has standardized relay technology in New Radio (NR) V2X sidelink to extend the transmission range under interference. In this paper, through a link-level and system-level simulation study, we evaluate the sidelink performance in relaying scenarios under different interference. Motivated by the recent success of deep learning, a novel neural network is further introduced as a unified benchmark for interference mitigation evaluation. Numerical results show that there exist challenges in the real-time optimization of transmission scheme selection and power allocation in relay-assisted cases. The simulation also reveals that the interference incurred by NR on unlicensed spectrum (NR-U) signals and other sidelink signals is intractable to be suppressed, which may bring potential challenges in future works.

Keywords: 5G NR, Interference identification, Neural network, Relay, Sidelink, V2X

1 Introduction

Nowadays, due to the rapid growth of autonomous driving and networked vehicle holdings, vehicle-to-everything (V2X) communication has been envisioned as one of the compelling technology for providing wireless connectivity to support the data exchange among vehicles and other network entities. The above vehicular connection technologies empower reliable connectivity with other vehicles (V2V) and roadside infrastructure (V2I). In this sense, connected vehicles have a potential advantage in reducing car crash accidents, traffic jams, and carbon footprint, etc. To meet the
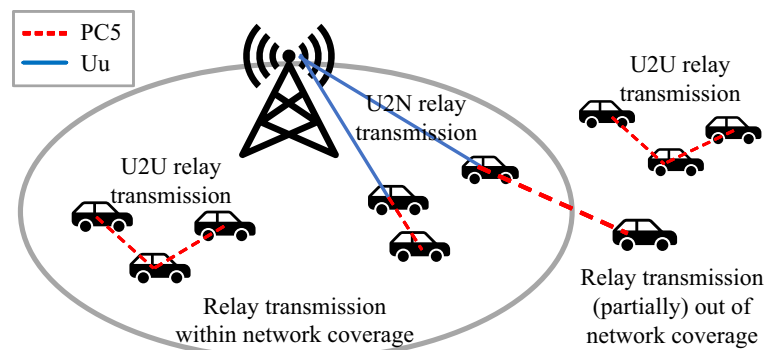
above requirements, two main radio access standards were developed to facilitate direct vehicular communications, i.e., dedicated short-range communication (DSRC) [1] and cellular V2X (C-V2X) [2]. The former one was built on IEEE 802.11p, while the newcomer was initially introduced by the Third Generation Partnership Project (3GPP) in its Release 14 (Rel-14) [3].

Over the last decade, DSRC has been the dominating technology for connecting vehicles. Derived from 802.11 standards, DSRC has similar physical (PHY) and medium access control (MAC) protocols, the effectiveness of which has been verified in Wi-Fi. Nevertheless, 802.11p suffers from some inherent defects such as a lack of effective quality of service (QoS) guarantees, unbounded delay control, and poor scalability issue [4]. In the urban traffic scenarios with high connection densities, several limitations like channel congestion and small communication radius hold it back from large-scale commercial deployments. In addition, it cannot provide consecutive V2I connectivity without pervasive roadside units (RSUs), resulting in poor adaptation in highways or rural areas.

Given that DSRC cannot meet the demand for connected vehicles in future, C-V2X, a cellular-based V2X technology, has been proposed. C-V2X consists of two extra links compared with DSRC, i.e., vehicle-to-pedestrian (V2P) and vehicle-to-network (V2N) links. With the help of cellular base stations (BSs), it can achieve broader coverage, higher reliability, and lower latency, as well as better QoS guarantees. Besides, it has the same evolutionary route as the mobile wireless communication techniques and thus can smoothly transit toward next-generation mobile communication. In that sense, safety and non-safety applications can be supported well in C-V2X. As aforementioned, 3GPP initiated the first standard in the Rel-14 [3], known as 4G Long Term Evolution (LTE) C-V2X. This standard was further upgraded to the Release-17 (Rel-17)[5], named 5G New Radio (NR) V2X.

NR C-V2X also introduces sidelink radio technology, known as the PC5 interface, into vehicle communication. In this way, a pair of user equipment (UE) can be directly connected and are assumed to work in an ad-hoc pattern. Additionally, two modes for radio resource management (RRM), i.e., Mode 1 and Mode 2, are designed to support V2V direct communications both in coverage and out of coverage of cellular BSs. Specifically, in Mode 1 control plane data is exchanged over the Uu interface, and radio resources are centrally allocated and scheduled by BSs. While in Mode 2, radio resources are autonomously selected and managed by UEs without the BSs' support. On this basis, NR C-V2X has been regarded as the most promising remedy to fulfill the requirements of the driving use cases in future.

Different from conventional cellular communications, V2X confronts a more complicated and dynamic radio environment due to mobility and limited available bandwidth. Several environmental factors like high propagation loss and mutual interference may impact the coverage areas and system performance. In this case, Rel-17 has introduced relay technology in sidelink, as illustrated in Fig. 1. More specifically, sidelink relay includes two typical applications, i.e., UE-to-Network (U2N) relay, and UE-to-UE (U2U) relay. The UE acts as the relay node that transfers data between remote users and infrastructure or two remote users, respectively. The work in [6] suggests that relays

Fig. 1 Communication modes of sidelink relaying

can expand communication coverage, mitigate interference, and enhance network throughput.

The 5.9 GHz band has been regarded as one of the most challenging spectrums since there exists a large number of applications that operate in both co-channel and adjacent channel bands, leading to either intra-system or inter-system interference. This band is first assigned to intelligent transportation system (ITS), so the DSRC can cause interference to C-V2X users operating in almost the same band range. In terms of inter-system interference, 3GPP has specially designed channel access technology in unlicensed spectrum, LTE Licensed-Assisted Access (LAA) [7], and NR-U [8], for example. Moreover, Wi-Fi devices that work in an adjacent band may also cause interference because of out-of-band emissions (OOBE), especially if such equipment is within a certain range of the sidelink transceiver. Interference above particularly plays a non-negligible role in sidelink relaying performance. To this end, it is necessary to investigate how significant signals of different protocols impact sidelink performance and then design the corresponding mitigating methods, notwithstanding there exist some proactive regulations such as listen-before-talk (LBT), maximum channel occupation time (MCOT), etc.

In this paper, through a link-level and system-level simulation study, we evaluate sidelink relaying performance in an urban scenario and provide direct insight into the challenges of optimizing overall communication performance. Further, we formulate a neural network as a unified measurement to classify interference signals of different protocols. The classification results indicate how difficult the specific interference is mitigated. In general, a signal that has lower classification accuracy suggests it is more challenging to be detected and then be suppressed in the mixed signals. The main contributions of this paper are summarized below.

- The existing 3GPP standards only consider the transmitting process but not the receiving. Here we first design the link-level simulation at the receiver to compare block error rate (BLER) performance at different modulation and coding schemes (MCSs). Subsequently, we use the physical layer abstraction (PLA) technology to formulate the system-level simulation and investigate the packet reception rate (PRR) and throughput in different scenarios.
- To our best knowledge, we are the first to propose a neural network-based signal recognition method to detect the interference signal protocol in the 5.9 GHz unli-

censed band. Almost all the existing works consider automatic modulation classification (AMC), which is not applicable in LTE and NR scenarios since the modulation schemes are only related to MCSs. In other words, different interference signals can have the same modulation schemes while signals of the same protocol usually have different modulation schemes.

The remainder of this paper is organized as follows. Related work is briefly reviewed in Sects. 2, and 3 details the simulation model. In Sect. 4, we introduce the proposed neural network. Then the simulation results and discussion are given in Sect. 5, followed by the conclusion in Sect. 6.

2 Related work

Over recent years, C-V2X sidelink communication has been largely studied, especially in the relaying scenarios. In this section, we provide an overview of the most relevant works on link-level simulation, system-level simulation, and signal identification.

To evaluate the performance of sidelink, most researchers implement link simulation to test physical layer technologies. In [9], the authors design an LTE V2X link simulator to analyze physical layer transmission performance on highways and obtain the performance curves of signal-noise ratio (SNR) and BLER at different vehicle speeds. In addition, Sattiraju et al. [10] investigate the BLER performance using IEEE 802.11p and LTE V2X. This work evaluates BLER performance with MCSs in the additive white Gaussian noise (AWGN) channel and with different SNRs in 5 kinds of V2V links. Anwar et al. [11] further utilize PLA to evaluate the BLER performance of LTE-V2X and NR V2X. The result of the PLA simulation is close to that of the real end-to-end link simulation. It is noted that the V2V link simulation in LTE V2X of work [9, 10] cannot accurately describe the link performance of NR V2X in most scenarios. [11] cannot directly reflect the impact of physical layer parameters on the BLER, notwithstanding it reduces simulation time and algorithm complexity.

As for the system-level simulation, the existing work mainly includes two aspects, i.e., U2N and U2U. Schellmann et al. [12] propose a corporative retransmission scheme in which BSs provide multiple isolated links to the target vehicle through adjacent vehicles. This scheme enables several times retransmission in the time budget and significantly improves transmission reliability. Further, Elbal et al. [13] use the stochastic geometric theory to derive a relay selection policy. It considers the distribution density of connected users and BSs to maximize signal coverage. In [14], Hu et al. use BLER and channel capacity to evaluate the performance of direct transmission and relay transmission in the ultra-reliable low latency communication (URLLC) network. It is noted that the above works are all focused on U2N applications. In the U2U scenario, Noor-A-Rahim et al. [15] further propose a relay scheme at the crossroad in urban to evaluate the broadcast performance of basic safety messages. The results show that the relay-assisted transmission scheme has significant system performance improvement compared to the direct transmission scheme. Moreover, Fu et al. [16] investigate the multicast relay policy based on sparse code multiple access (SCMA) in the vehicle fleet, indicating that the use of a relay transmission scheme can compensate for the path loss and reduce the

average outage of the system. Nevertheless, the research in [12–14] derives the analytical expression based on a simplified system model, which may not adapt to the real scenes. Besides, the simulation in work [15, 16] just considers the path loss, ignoring the small-scale fading.

All of the above methods, however, are faced with the predicament of multiple interferences. Gaurang et al. [17] have demonstrated that C-V2X is at risk from Wi-Fi operations in the adjacent bands and existing mechanisms are also not suitable to coexist with Wi-Fi. Besides, Shao-Yu et al. [18] analytic models for four types of multi-band channel access procedures in 3GPP NR-U and LTE LAA to capture both inter-system and intra-system interference from coexisting Wi-Fi transmitters and V2X transmitters. Thereby, sidelink users may be susceptible to interference from both co-channel and adjacent channels. In terms of interference identification, there has been a large amount of research based on neural networks. [19] firstly introduce convolutional neural networks (CNNs) to signal recognition. The work in [20] further use long short-term memory (LSTM) networks to recognition. Then, Zhang et al. [21] combined the advantages of these two networks to extract signal features. The above works are all focused on AMC and only a few works research protocol detection. Moreover, [22] have implemented interference identification in ISM band based on CNN. The work in [23] investigated interference recognition of cellular signals operating at licensed spectrum based on CNN. None of the above works have studied interference identification at unlicensed spectrum at 5.9 GHz.

Different from the above existing works, in this paper, we evaluate the sidelink relaying transmission scheme in a non-line of sight (NLoS) scenario at a crossroad with the consideration of both large-scale and small-scale fading. Furthermore, we formulate an interference identification neural network as a benchmark to analyze the mitigation difficulties of different interference on sidelink signals.

3 Methods and system model

In this section, we formulate our system model, in which a two-level simulation method is proposed, i.e., link-level and system-level simulation. We initially go to the details of the protocol analysis in receive link in the first subsection. Then, we model a sidelink communication network where different interferences exist in the vehicle relay scenario. Along the way, the main notation used in the paper will also be introduced.
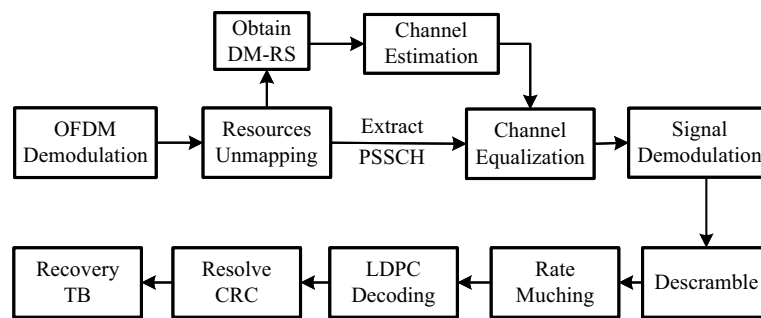
3.1 Link-level simulation model

In what follows, we emphasize the performance evaluation on the physical layer. To realize flexible deployment in diverse scenarios, C-V2X supports multiple MCSs in both frequency range 1 (FR1) and frequency range 2 (FR2), resulting in different subcarrier spacing (SCS) and cyclic prefixes (CPs). It is notably necessary to evaluate the link performance when NR sidelink utilizes different MCSs, to prepare for the system-level simulation.

As explained before, NR sidelink supports some new features such as multicast and hybrid automatic repeat request (HARQ). To support such features, two sub-channelization channels are designed in NR sidelink, i.e., physical sidelink shared channel (PSSCH) and physical sidelink control channel (PSCCH). Similar to the physical

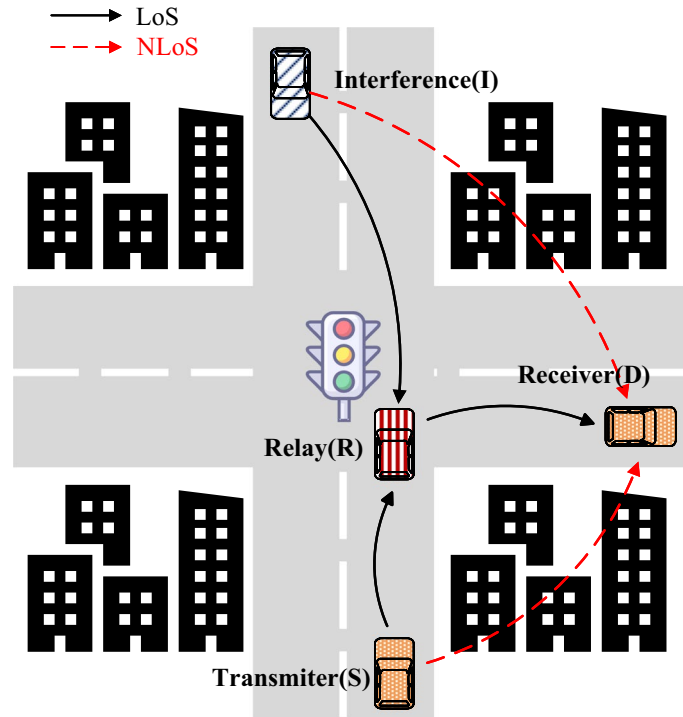**Fig. 2** Sketch map of the PSSCH time-frequancy structure

Fig. 3 Receiving link of PSSCH

channel of basic NR signals, each channel is split into multiple frames in the time domain and multiple subchannels in the frequency domain. Each frame consists of multiple subframes and then, slots. Figure 2 illustrates single resource blocks (RBs) in NR sidelink, which contains 14 OFDM symbols and integrates PSSCH and PSSSH. Note that the first symbol is designed for automatic gain control (AGC) as the status of transceivers and signal strength in each slot varies dynamically. Meanwhile, the last symbol is used to provide a guard period (GP) for transmission and receive status switch. Demodulation reference signals (DM-RS) of diverse designs are in comb-link distribution and contain channel information. It is worth mentioning that based on whether or not contains a physical sidelink feedback channel (PSFCH), there exist two kinds of structures in sidelink. To simplify the discussion, we only focus on the basic one, as depicted in Fig. 2.

Based on the above considerations and transmit procedure defined in 3GPP standards [24–26], here we design the link-level simulation model at the receiver. We suppose that every frame that arrived has been perfectly synchronized and demodulated, as well as the frequency offset has been perfectly estimated and compensated. In this case, the signal is processed sequentially as depicted in Fig. 3. Specifically, the DM-RS and PSSCH are firstly extracted through OFDM demodulation and resource unmapping. Then, we use the least squares (LS) and minimum mean square error (MMSE), respectively, to implement channel estimation and equalization, according to the knowledge obtained from DM-RS. Subsequently, the signal is demodulated based on

Table 1 Path loss channel models in different transmission types

Transmission types	Path loss (dB)	SD
LoS	$PL = 32.4 + 20 \log_{10}(d) + 20 \log_{10}(f_c)$	$\sigma_{SF} = 3$
NLoS	$PL = 36.85 + 30 \log_{10}(d) + 18.9 \log_{10}(f_c)$	$\sigma_{SF} = 4$

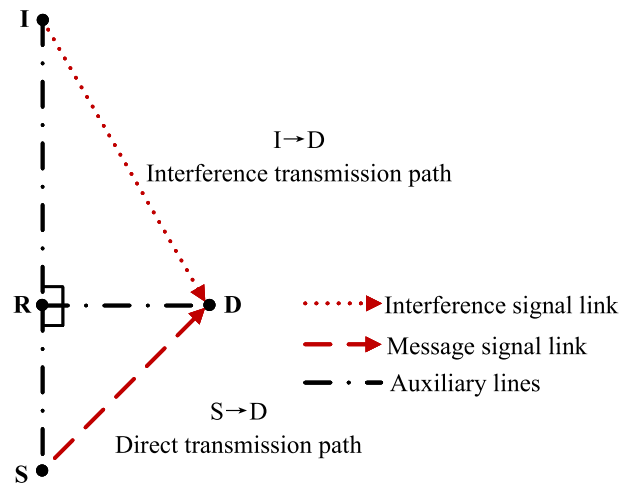**Fig. 4** Sketch map of V2X communication at the crossroad

the maximum posterior log-likelihood ratio (LLR), and then descramble. Eventually, the remaining modules implement rate matching, decoding, etc.
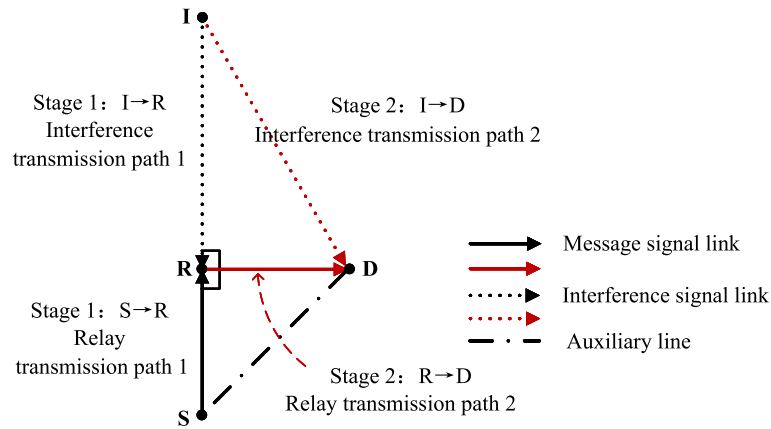
3.2 System-level simulation model

The sidelink transmission is likely to be interrupted due to the densely distributed construction and extremely complicated transportation system in cities. One of the typical scenarios in NLoS communication is the crossroads. Without loss of generality, we consider the system-level simulation in a crossroad mode and investigate whether a relay node can yield better system performance.

As illustrated in Fig. 4, we assume that the transmitter at vehicle *S* and receiver at vehicle *D* are distributed on two crossing roads, respectively. The communication may be limited since the buildings among them shadow the line of sight (LoS) path. To address this issue, we consider introducing a relay node to expand the communication distance and improve reliability without increasing the transmitting power budget. For example, a vehicle *R* at the center of the crossing can be chosen as the relay and thus decompose the NLoS communication into two LoS communication processes. Furthermore, in the above scenario, there might be interference from either the sidelink signal or any other

Fig. 5 Direct transmission system model

Fig. 6 Relay transmission system model

signal such as NR-U, LTE LAA, Wi-Fi, etc. We assume the interference, if exists, coming from a vehicle *I* existing at the remote. The details of the model for interference detection and impact assessment will be further discussed in Sect. 4.

In the following discussion, for simplicity, we ignore the vehicle size and street width. Each vehicle and street is presented as a point and line, respectively. Besides, we assume that vehicle *S* and vehicle *D* have the same distance to the center of the crossing, and that vehicle *I*, vehicle *R*, and vehicle *S* are approximately on the same line. Under this condition, four vehicles compose two right triangles, as depicted in Figs. 5 and 6. In this scenario, let the signal $\boldsymbol{x}_X$ be the vector of symbols transmitted by vehicle *X*, and $\boldsymbol{H}_{X,Y}$ be the frequency channel matrix that the signal goes through. Here we also define $P_{X,Y}$ as the signal power transmitted by vehicle *X* and received by vehicle *Y*, respectively. In this way, we adopt the model [27] designed for V2V transmission at 5.9 GHz as the small-scale fading model and employ the model defined in [28] as the large-scale fading model, which is defined in Table 1.

Firstly, we consider the situation when lack of delay. In terms of direct transmission, the mth subcarrier vehicle D receives can be defined as

$$\boldsymbol{y}_{S,D}(m) = \sqrt{P_{S,D}}\boldsymbol{H}_{S,D}(m)\boldsymbol{x}_S(m) + \sqrt{P_{I,D}}\boldsymbol{H}_{I,D}(m)\boldsymbol{x}_I(m) + \boldsymbol{n}(m) \tag{1}$$

where n is the noise power with variance N_0. Then, the signal to interference and noise power ratio (SINR) can be presented as

$$\gamma_{S,D}(m) = \frac{P_{S,D}|\boldsymbol{H}_{S,D}(m)|^2}{P_{I,D}|\boldsymbol{H}_{I,D}(m)|^2 + N_0} \tag{2}$$

where path loss and shadow fades have been taken into consideration.

On the other hand, a relay node can decompose the process into two stages, as depicted in Fig. 6. In the first stage, vehicle S transmits signals to vehicle R, which is similar to the direct transmission mentioned before. Vehicle R, in the second stage, transfer the received signal to vehicle S. Please note that all the receiver in the relay transmission scheme will be affected by interference.

In the first stage, the mth subcarrier vehicle R receives can be defined as

$$\boldsymbol{y}_{S,R}(m) = \sqrt{P_{S,R}}\boldsymbol{H}_{S,R}(m)\boldsymbol{x}_S(m) + \sqrt{P_{I,R}}\boldsymbol{H}_{I,R}(m)\boldsymbol{x}_I(m) + \boldsymbol{n}(m). \tag{3}$$

Similarly, as for the vehicle R, the SINR of the received signal can be defined as

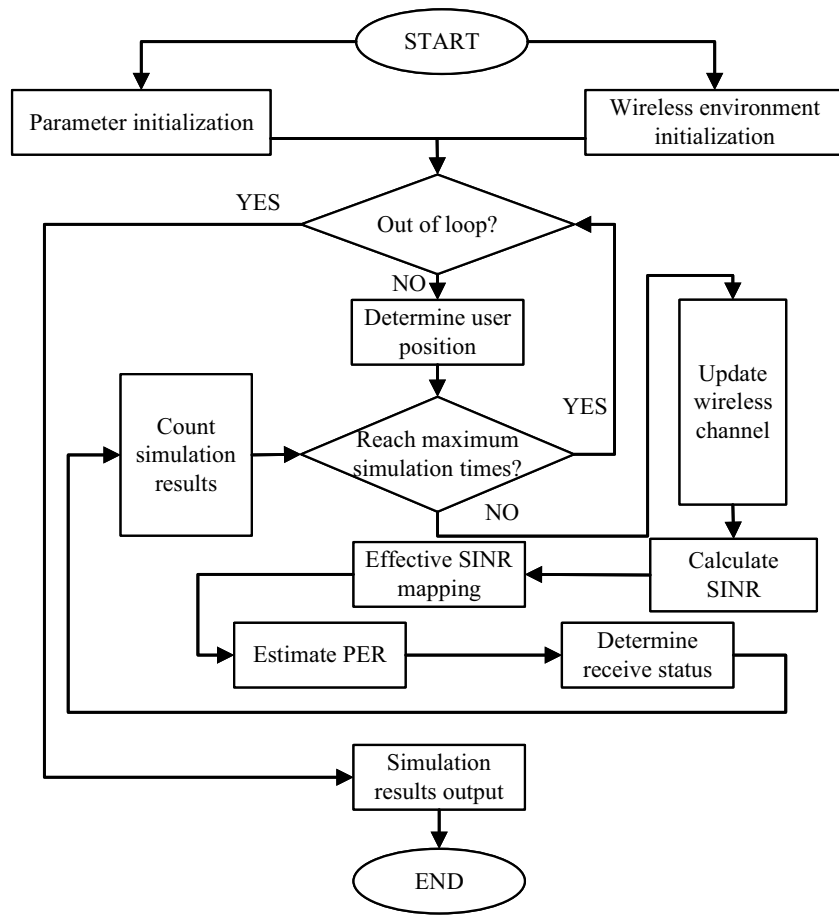$$\gamma_{S,R}(m) = \frac{P_{S,R}|\boldsymbol{H}_{S,R}(m)|^2}{P_{I,R}|\boldsymbol{H}_{I,R}(m)|^2 + N_0}. \tag{4}$$

In the second stage, vehicle R transfers the received signal from vehicle S and it is easily concluded that the mth subcarrier vehicle D receives can be defined as

$$\boldsymbol{y}_{R,D}(m) = \sqrt{P_{R,D}}\boldsymbol{H}_{R,D}(m)\boldsymbol{x}_R(m) + \sqrt{P_{I,D}}\boldsymbol{H}_{I,D}(m)\boldsymbol{x}_I(m) + \boldsymbol{n}(m). \tag{5}$$

Likewise, the SINR of vehicle D is

$$\gamma_{R,D}(m) = \frac{P_{R,D}|\boldsymbol{H}_{R,D}(m)|^2}{P_{I,D}|\boldsymbol{H}_{I,D}(m)|^2 + N_0}. \tag{6}$$

To simplify the discussion, here we use the PLA technique to provide an application interface between link-level and system-level simulation. Specifically, the simulation procedure is listed in Fig. 7. Initially, the simulation environment is set up according to the preset parameters such as channel bandwidth, user MCS, and channel model. We randomly spread users and determine the position of the four vehicles based on the above discussion. To guarantee the reliability of the numerical results, each user transfers up to one hundred thousand times of data packets at a single position and then moves to the next position. Subsequently, every time the user, i.e., vehicle S, transmits data, the wireless channel is updated and the receiver at vehicle R or vehicle D will use the large-scale fading model to obtain the power of the target signal and interference signal received. In this process, the ideal channel matrix that the target signal and interference signal experience will also be obtained. Thus, we have

Fig. 7 Flowchart of system-level simulation

$$P_{\text{RX}}^{\text{TX}} = P_{\text{TX}} - PL \tag{7}$$

where P_{TX} is the signal power at the transmitter and PL presents large-scale fading. Next, UE calculates SINR $\{\gamma_i\}$ of each subcarrier according to (2)(4)(6), taking the relative position, interference, and fading into consideration. In what follows, PLA mentioned above is applied to operate effective SINR mapping (ESM). Since the physical channel has a different impact on different subcarriers in OFDM, it is necessary to map multiple $\{\gamma_i\}$ to a single effective SINR γ_{eff} and then search for the corresponding packet error rate (PER). The SINR mapping function can be expressed as

$$\gamma_{\text{eff}} = \alpha \cdot \Phi^{-1}\left\{\frac{1}{N}\sum_{i=1}^{N}\Phi\left(\frac{\gamma_i}{\beta}\right)\right\} \tag{8}$$

where $\Phi(\cdot)$ is the mapping function and N is the number of subcarriers. α and β are the indexes that control the MCS and channel coding rate. As mentioned in [11], in our research, we use the function $\Phi(\gamma_i; M)$ based on received bit mutual information (RBIR) to map the γ_{eff}. We have

$$\Phi(\gamma_i; M) = \log_2 M-$$
$$= \frac{1}{M} \sum_{m=1}^{M} E_U \left\{ \log_2 \left(\sum_{k=1}^{M} exp \left[\left(|U|^2 - \left| \sqrt{\gamma_i}(s_k - m_k) + U \right|^2 \right) \right] \right) \right\} \qquad (9)$$
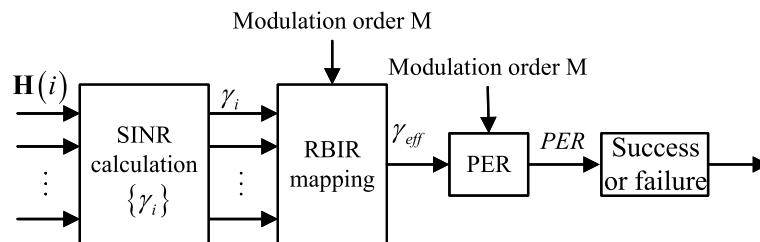
where $U \sim CN(0, 1)$ is a complex Gaussian random variable and M is modulation order. In practice, [29] provides RBIR mapping numbers for different modulation orders. At last, we use the γ_{eff} to search for the corresponding PER at the performance curve in Fig. 8 and judge whether the transmission is successful.

4 Neural network architecture

As aforementioned, C-V2X operates on the 5.9 GHz band and is susceptible to both co-channel and adjacent channel interference. Additionally, some of the recent research has demonstrated that the wireless communication technology work on the unlicensed band is the major cause for the interference because of the OOBE. To this end, it is important to investigate to what extent different signals affect the sidelink performance and evaluate the handling difficulty.

Based on the above considerations, a unified criterion is required to evaluate the interference impact. Nevertheless, the signal of different protocols may have the same modulation schemes and similar structures. So it is significantly difficult to design a model-based method to analyze the impact of different interference signals and the difficulty of mitigation. On this basis, data-driven schemes may provide a promising solution to this problem. Since the same neural network has the same expression ability for different signals, its classification results can provide a benchmark for interference evaluation. The interference signal that has lower classification accuracy is likely more difficult to be detected and thus mitigated.

Note that the MCSs of the same signal can be dynamic and different modulation schemes can be utilized simultaneously in a single sampling time. In this subsection, we propose a novel neural network to classify the signal based on their protocol, rather than modulation. Different from the modulation scheme, the characteristics of protocols are easier to be destroyed and extremely difficult to be detected when multiple signals coexist. In general, sequence signal processing is synonymous with recurrent neural networks (RNNs) like LSTM. CNNs are usually seemed to be effective at extracting complicated features and patterns from large amounts of data, while RNNs are adept at extracting the relationships from time-dependent sequential data. However, a famous work [30] has conducted a systematic evaluation of convolutional and recurrent architectures for sequence modeling, indicating that a simple CNN can
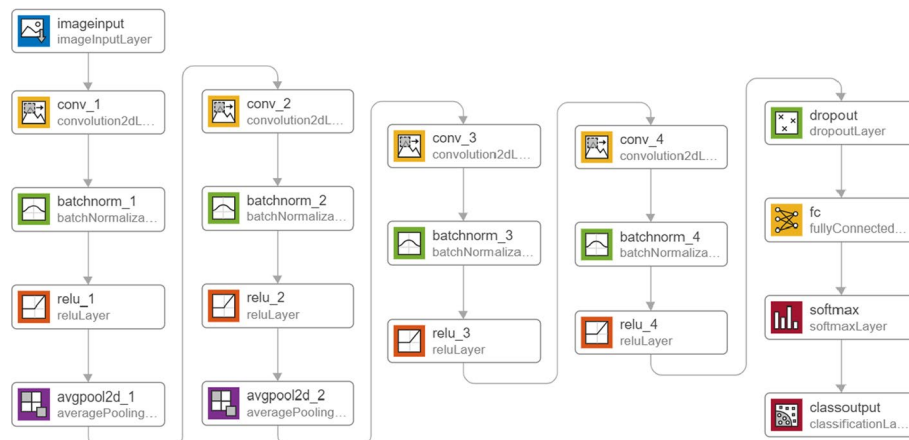

Fig. 8 Flowchart of PER prediction based on RBIR

outperform canonical RNN in some specific tasks. This is because CNNs have parallel inference, flexible receptive field size, stable gradients, and low memory requirement for training. Chen et al. [31] also compares the performance of RNN and CNN, concluding that CNNs are more suitable for interference identification. Actually, the majority of the existing work about signal identification is based on CNNs or more complicated CNN-LSTM combinations. This is due to the frame structures are similar in the time domain, making it more important to effectively extract features from the complex mixed-signal itself than from the time domain.

It is noted that we only regard the neural network as an evaluation measurement in this work and do not concentrate on network optimization or performance comparison. For the sake of simplicity, our proposed network is based on CNN. The main architecture is illustrated in Fig. 9. Specifically, it is a typical convolutional neural network that includes four convolutional layers, each followed by batch normalization, ReLU activation function layer, and average pooling. Note that the size of the input layer is pre-designed as $128 \times 300 \times 2$ to be consistent with the dimension of the transformed signal in the following. Then, we design the filter size as 3×3 and the filter numbers are set to 8 and 16, respectively, for the first two layers and 32 for the last two layers. Besides, the pool size is 2×2 with 2 strides and the dropout layer has a 0.4 drop rate. At last, the output layer uses the dense layer and softmax function to output classification results.

To make the signal consistent with the input of the neural network, short-time Fourier transform (STFT) has been adopted to transform the signals into a time-frequency distribution matrix, which contains the features of frequency varying with time. This implementation transforms the one-dimension raw signal to two-dimensions inputs and enable the CNN to become sensitive to the time order. The transformation can be expressed as

$$X_m(f) = \sum_{n=0}^{Nx} x(n)g(n - mR)e^{-j2\pi fn}.$$ (10)

Fig. 9 Framework of the proposed neural network

Specifically, the received signal $x(n)$ is processed by a sliding window $g(n)$ of length M. The Fourier transformation is implemented in each time segment, thereby the two-dimensional function of time-frequency can be solved by cascading the above transformation results sequentially. Since the signal degrades significantly at the edge of a sliding window, we define an overlap of length L to compensate for such attenuation and the slide distance each time is thus $M - L$. Let the total length is N_x, we have

$$k = \lfloor \frac{N_x - L}{M - L} \rfloor \tag{11}$$

where k is the time dimension length of STFT. Moreover, a resampling implementation is required before being fed into networks, since the input size of CNN is fixed while series data of different protocols often have variable sizes. Note that the input of CNN is limited to real value. To reserve the amplitude and phase information comprised in the complexed value, we further present the signal with two dimensions, thus expanding the time-frequency matrix to three dimensions.

5 Simulation results and discussion

In this section, through a comprehensive and systematic simulation study, we investigate the potential challenges in V2X sidelink relaying. The results of both link-level and system-level simulations provide some direct insight into parameter optimization and interference mitigation.

5.1 Link-level simulation

We take a look at the link performance of NR sidelink in this subsection. We use the Simulink® in MATLAB® 2021b to construct the simulation link and then analysis the BLER performance of PSSCH in the AWGN channel. Simulation parameters are set according to the 3GPP TS38.101 [32], some of which are tabulated in Table 2. Moreover, 3GPP TS38.214 has defined 28 MCSs and without loss of generality, we have 8 MCSs out of them in this simulation. Note that when calculating the SNR through IFFT, we should take empty subcarriers into consideration. Otherwise, the noise received in practice would be degraded since the noise is additive to all symbols while the number of effective subcarriers may not identical to that of IFFT points. SNR_{real} in link simulation can be defined as

Table 2 Parameters of link-level simulation

Paramaters	Values
System bandwidth	10 MHz
Subcarriers spacing	15 kHz
Transport block size	190 Bytes
MCSs	MCS1/MCS3/MCS5/MCS8: QPSK
	MCS11/MCS13: 16QAM
	MCS19/MCS25: 64QAM
Numbers of RBs occupied by MCSs	46/30/21/15/13/11/8/6
Number of simulations	100000 transport blocks

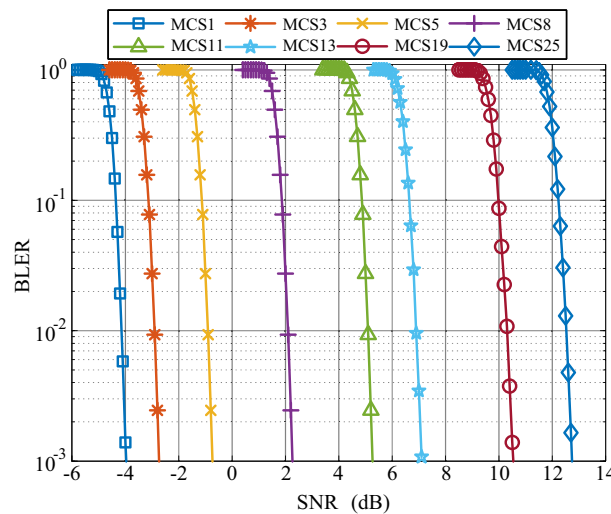$$SNR_{\mathrm{real}} = SNR - 10\log_{10}\frac{N_{\mathrm{IFFT}}}{N_{\mathrm{st}}} \tag{12}$$

where N_{IFFT} is the number of IFFT points and N_{st} presents the number of effective subcarriers.

Figure 10 illustrates the comparison of different MCSs with BLER versus SNR. It indicates that given the same BLER requirement, the corresponding SNR threshold increases with the index of MCS increasing. Users generally adopt different MCSs to obtain promising transmission rates according to current SNR and radio resources. Further, we note that in some cases the radio environment is so poor that SNR is just -6 dB and the BLER cannot reach 10^{-2} even if the receiver works at MCS1. In such cases, introducing a relay node may improve communication reliability.

5.2 System-level simulation

System-level simulation can evaluate communication systems on some indicators like transmission distance and throughput with less time and compute requirement compared with end-to-end simulation at the link level. The system-level simulation can be roughly divided into two parts. In the first part, we investigate whether and how much signals of multiple protocol impact sidelink performance. Then in the second part, we evaluate the PRR and user throughput of the system in two situations, i.e., with and without interference.

As aforementioned, we proposed a novel neural network to detect different interference. This method does not demand any prior knowledge since neither demodulation nor decoding is required in the preprocessing. We mainly consider the signal operates in the unlicensed band such as NR-U, LTE LAA, Wi-Fi, and Bluetooth and generate them. For each kind of signal, we define some specific characteristics such as channel bandwidth, MCS, and allocated RBs. The generated signals are summarized in Table 3. Specifically, to unify the signal number of different protocols, we generate

Fig. 10 BLER performance versus SNR in the AWGN channel

Table 3 Parameters of waveform generation

Protocols	Parameters	Values
NR-U	Frequency range	Unlicensed band in 450MHz-6GHz
	Subcarriers spacing	15/30/60 kHz
	Modulation schemes	QPSK/16QAM/64QAM/128QAM
	Channel bandwidth	5/10/15/20/25/30/40/50 MHz
	Duplex mode	FDD/TDD
LTE LAA	Reference channels [35]	R.1/R.2/R.3/R.4/R.5/R.6/R.7/R.8/R.9/R.10
		R.11/R.12/R.13/R.14/R.25/R.26/R.27/R.28
		R.313A/R.314/R.43/R.44/R.45/R.451/R.48/R.50
		R.51/R.6-27RB/R.12-9RB/R.11-45RB
	Modulation schemes	QPSK/16QAM/64QAM/128QAM
	Numbers of RBs occupied	100/75/50/39/27/25/15/6/1
	Duplex mode	FDD/TDD
	Coding schemes	BCC/LDPC
Wi-Fi	Modulation schemes	BPSK/QPSK/16QAM/64QAM/256QAM
	Guard interval	Short/long
	Channel bandwidth	20/40/80/60 MHz
Bluetooth	Data rates	125/500/1M/2M bps

the signal with each segment lasting 10ms and resample it to 3.84 M samples/s, which means each segment contains 38400 sample points. To emulate the actual scene where the sidelink signal interfered, we assume that NR-U, LTE LAA, Wi-Fi, and Bluetooth are interference signals and mix them with the sidelink signal, respectively. For every kind of signal, we generate 1000 segments thus the dataset contains 5000 mixing signals in total. The training set and test set are divided by 8:2.

Before being fed into the network, the data are preprocessed to transfer 38400 sample points in each segment to a time-frequency matrix with the size of 128×300, through the STFT mentioned in Sect. 4. The SGDM is chosen as the optimizer. We use a batch size of 128 and train the networks for 25 epochs. The initial learning rate is $1.25e^{-4}$ and will finally drop to $1.25e^{-5}$. The model is validated on the local server, with Intel® Core i7-8700K CPU and MATLAB®.
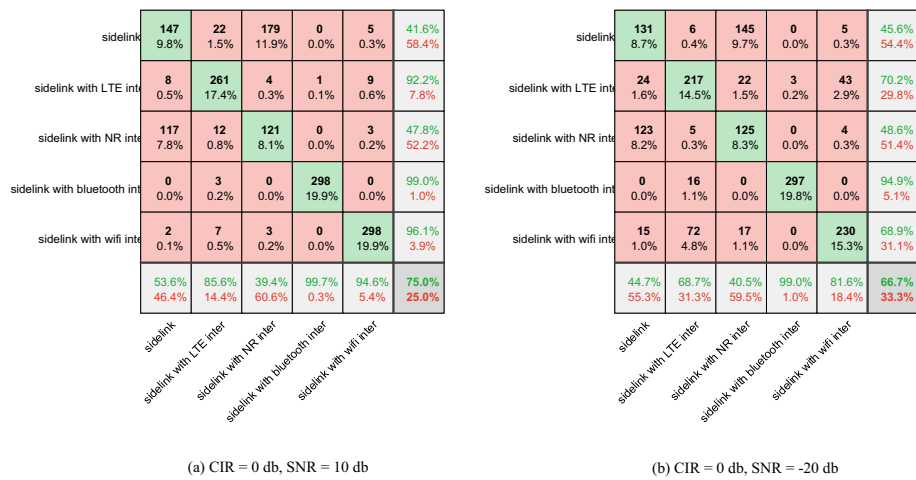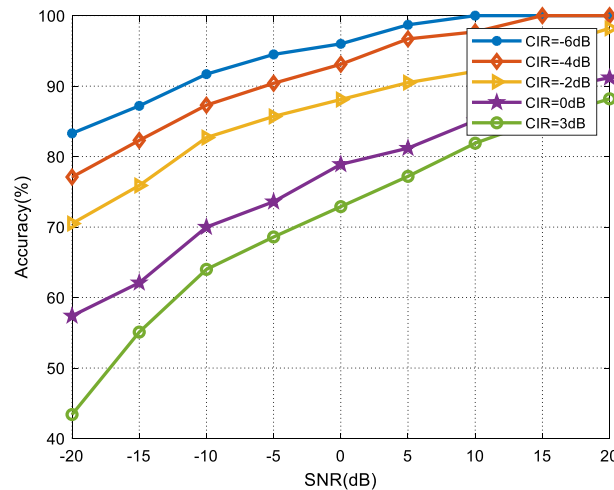
The output result is depicted in Fig. 11 as confusion matrixes. On the confusion matrix plot above, the rows correspond to the predicted class and the columns correspond to the true class. The diagonal cells correspond to observations that are correctly classified, while others correspond to incorrectly classified observations. Accordingly, the column on the far right of the plot shows the precision and the row at the bottom of the plot shows the recall. The cell in the bottom right of the plot presents the overall accuracy.

From Fig. 11a, we can easily see that Bluetooth is the easiest to be detected, followed by Wi-Fi signals. LTE LAA is somewhat identical to sidelink and thus the precision and recall may be impacted in some cases. It is worth noting that the network has the worst performance on NR-U since both the precision and recall are close to 50%, which means it nearly cannot detect any of the interference incurred by NR-U. We conclude that this is because NR sidelink is designed based on the basic NR signal and has the most identical protocol. Compared with Fig. 11a, b shows that the reduction

Table 4 Parameters of system-level simulation

Paramaters	Values
Center carrier frequency	5.9 GHz
Subcarriers spacing	15 kHz
MCSs	MCS1/MCS5/MCS13/MCS25
Transmission path	LoS/NLoS in urban
Total transmitting power	$\leq$ 23 dBm
Interference power	23 dBm
Noise Figure	9 dB
Number of simulations	100000 data packets

(a) CIR = 0 db, SNR = 10 db   (b) CIR = 0 db, SNR = -20 db

Fig. 11 Confusion matrix of the network output with CIR = 0, − 2 dB when SNR = 10 dB

Fig. 12 Classification accuracy at different SNRs

in carrier-to-interference ratio (CIR) leads to relatively high detection performance. Since the NR signals significantly impact classification accuracy, we remove them from the dataset to evaluate the impact of SNR and CIR. It is not surprising as we

can see more obviously from Fig. 12 below that the accuracy is increasing with SNR increasing and CIR reducing. The reason is that when the strength of the interference signal is large, the characteristic difference between multiple signals is obvious, which leads to greater detection performance. On the contrary, lower SNR induces the characteristic merged in the noise, leading to poorer classification accuracy.

In summary, the above analysis indicates that different interference has a notably different impact on sidelink signal, as Bluetooth and Wi-Fi are easier to be detected while NR-U is extremely intractable when mixed with NR sidelink. Furthermore, it also suggests that in scenarios with different CIR and SNR, different interference mitigation measures may be considered. Please note that the neural network proposed is absolutely not state-of-the-art, but it provides a uniform standard for us to evaluate the impact of diverse interference on sidelink signals in different channel environments.

As explained above, we have proposed a method to detect the existence of different interference. On this basis, in the following, we use the system model defined in Sect. 3 to compare direct transmission and relaying schemes in both interference scenarios and interference-free scenarios. The distance between vehicle S and vehicle D ranged from 60 to 420 m. In each position, we transmit data packets 100 thousand times. Here, the PRR of vehicle D is defined as the main indicator to evaluate the system reliability, that is
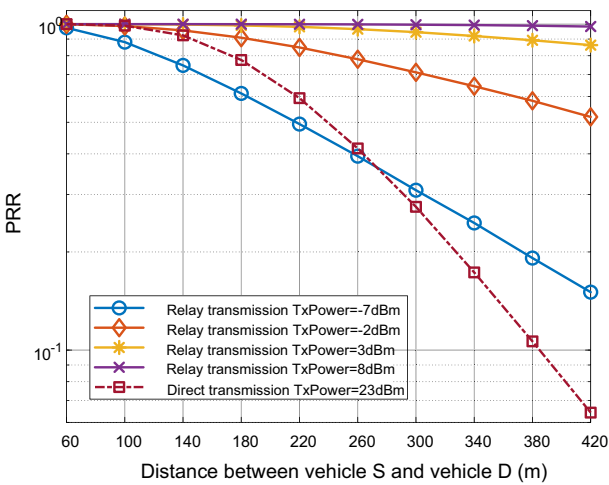
$$PRR = \frac{N_{\text{correct}}^{\text{Rx}}}{N_{\text{total}}^{\text{Tx}}} \tag{13}$$

where $N_{\text{correct}}^{\text{Rx}}$ and $N_{\text{total}}^{\text{Tx}}$ is the number of correct decoding data packets and packets transmitted in total, respectively. Throughput can be
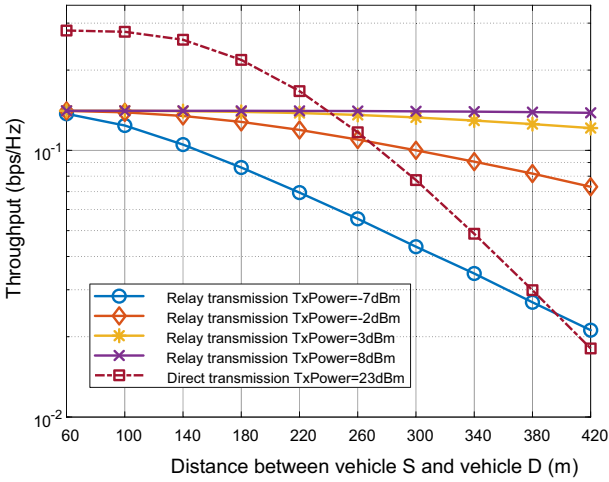
$$\Theta = \frac{N_{\text{correct}}^{\text{Rx}} \cdot B}{T_{\text{total}} \cdot w_{\text{total}}} \tag{14}$$

where B is the packet size, T_{total} is the total transmission time, and w_{total} is the user bandwidth. Furthermore, to ensure equality among the two schemes, the total transmission power of the relay scheme does not exceed the power of the direct transmission scheme, i.e., 23 dBm. The simulation parameters are listed in Table 4.
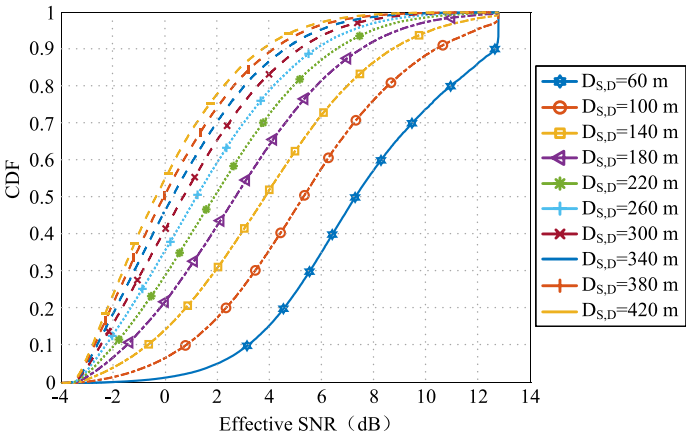
As illustrated in Fig. 13, three kinds of relay schemes outperform direct transmission in all distances, with higher PRR and less power required. Note that when P_{tx} of the relay scheme is -7 dBm, direct transmission at a short distance outperforms the former when the distance is lower than 270 m. However, this is due to the higher transmission power of direct transmission offsets the attenuation in NLoS. In practice, the relay scheme can choose significantly lower power to achieve the given PRR requirement. In Fig. 14, we conclude that the relay scheme only outperforms direct transmission at a long distance. This is probably because the throughput is influenced by the total transmission time. Compared with the direct transmission scheme, the processing time is almost 2 times in the relay scheme as the transmit delay exists in the relay node. However, there may be a threshold since the throughput of direct transmission degrades dramatically after 260 m, while a larger distance makes the throughput less susceptible to relay transmit delay. To

Fig. 13 PRR performance without interference

Fig. 14 Throughput performance without interference
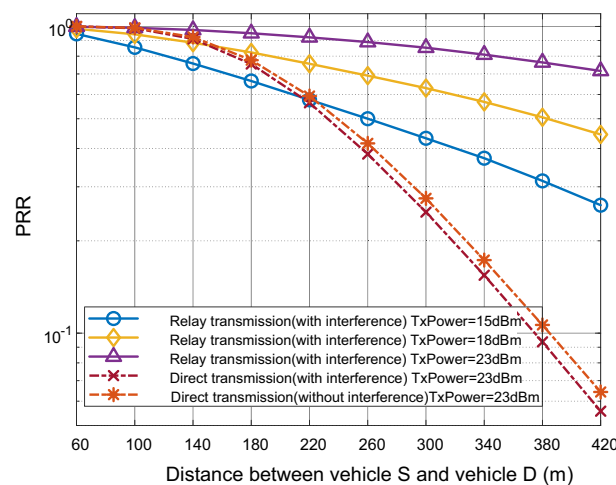

Fig. 15 CDF versus effective SNR at different distance without interference

this end, the relay selection may depend on the communication distance when taking throughput into consideration.
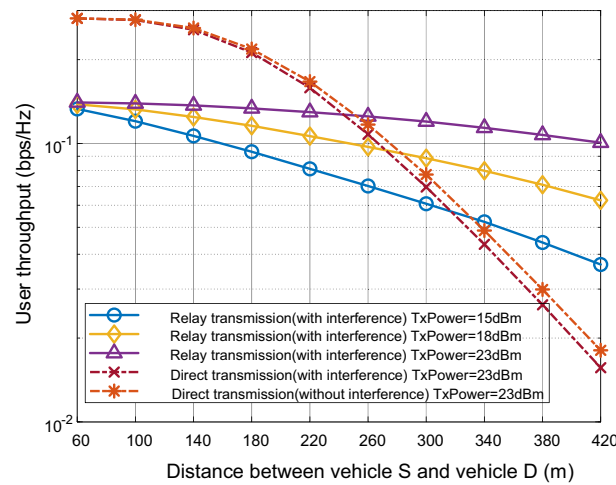
From the discussion above we have seen that it is necessary to determine when to start using relays. To address this issue, we introduce the cumulative distribution function (CDF) to describe the distribution of SINR γ_{eff}. Figure 15 illustrates the situation when $P_{\text{tx}} = -2$ dBm. We can easily find that given a CDF requirement of specific SINR γ_{eff}, there exists a threshold in distance, which is the last opportunity to start a relay transmission.

In the scenario where interference cannot be ignored, we assume that the distance between vehicle *I* and vehicle *D* is constantly 500 m and the normalized power of interference is 23 dBm. In Fig. 16, we see that interference has less impact on direct transmission as PRR is just 0.0126 lower than that without interference with a distance of 380 m. That is because interference also experiences NLoS channel hence the power is largely attenuated. Figure 16 below also illustrates that the relay scheme outperforms the direct transmission scheme in most of the scenarios. But in some cases, $P_{\text{tx}} = 15$ dBm and 18 dBm, for example, direct transmission has better performance, especially at a small distance. This is due to the interference signal experiencing LoS channel to vehicle *R* at stage one, reducing the receiving SNR of it. To this end, we suggest slightly increasing the transmit power of vehicle *S* to improve PRR. Similarly, Fig. 17 also indicates that interference has less impact on direct transmission while has a greater influence on the relay transmission scheme at a small distance. Thus, we tend to select the direct transmission scheme when at a small distance to obtain considerable throughput.

To conclude, it is intractable to mitigate some specific interference signals mixed in the NR sidelink signals. Our simulation results have also shown that the sidelink relay transmission is, in some sense, a complicated scenario. It is challenging for a connected vehicle to decide whether to implement direct transmission or relay transmission. Another consideration is how to select the optimal relaying vehicle and then negotiate with it to act as a relay node. Moreover, how to properly allocate powers

Fig. 16 PRR performance with interference

Fig. 17 Throughput performance with interference

to satisfy the selected transmission scheme while minimizing interference to others is also challenging. In this sense, the deep reinforcement learning (DRL) may provide a promising method to optimize the resource scheduling strategy. For example, a incentive-driven DRL method can be used to implement relay selection [33]. Further, unmanned aerial vehicles (UAVs) with reconfigurable intelligent surface (RIS) technology can also act as relay nodes in future to maximize the system capacity while reduce the power consumption [34].

6 Conclusion

In this paper, we have implemented link-level and system-level simulations to investigate parameter optimization and performance evaluation in the C-V2X sidelink relaying scenario. Furthermore, we propose a novel neural network to classify multiple interference signals by protocol detection. The simulation results provide direct insight into the system performance in relaying scenarios and reveal some challenges. For example, how to identify the interference incurred by NR-U and then mitigate it. Further, transmission scheme selection, relay selection and resource allocation are also challenges when there exist multiple relays and UEs. This may could be extended in future research.

Abbreviations

3GPP	Third Generation Partnership Project
C-V2X	Cellular vehicle-to-everything
NR	New Radio
NR-U	NR on unlicensed spectrum
V2X	Vehicle-to-everything
V2V	Vehicle-to-vehicle
V2I	Vehicle-to-infrastructure
DSRC	Dedicated short-range communication
PHY	Physical
MAC	Medium access control
QoS	Quality of service
RSU	Roadside unit
V2P	Vehicle-to-pedestrian
V2N	Vehicle-to-network
BS	Base station
LTE	Long Term Evolution

UE	User equipment
RRM	Radio resource management
U2N	UE-to-Network
U2U	UE-to-UE
ITS	Intelligent transportation systems
LAA	Licensed-Assisted Access
OOBE	Out-of-band emissions
LBT	Listen-before-talk
MCOT	Maximum channel occupation time
BLER	Block error rate
MCS	Modulation and coding scheme
PLA	Physical layer abstraction
PRR	Packet reception rate
SNR	Signal-noise ratio
AWGN	Additive white Gaussian noise
URLLC	Ultra-reliable low latency communication
SCMA	Sparse code multiple access
NLoS	Non-line of sight
FR1	Frequency range 1
FR2	Frequency range 2
SCS	Subcarrier spacing
CP	Cyclic prefix
HARQ	Hybrid automatic repeat request
PSSCH	Physical sidelink shared channel
PSCCH	Physical sidelink control channel
RB	Resource block
AGC	Automatic gain control
GP	Guard period
DMRS	Demodulation reference signal
PSFCH	Physical sidelink feedback channel
LS	Least squares
MMSE	Minimum mean square error
LLR	Log-likelihood ratio
LoS	Line of sight
SINR	Interference and noise power ratio
ESM	Effective SINR mapping
PER	Packet error rate
RBIR	Received bit mutual information
BP	Back propagation
LSTM	Long short-term memory
CNN	Convolutional neural network
STFT	Short-time Fourier transform
CIR	Carrier-to-interference ratio
CDF	Cumulative distribution function
DRL	Deep reinforcement learning
UAV	Unmanned aerial vehicle
RIS	Reconfigurable intelligent surface

Author contributions
All the authors contributed to the paper. All authors read and approved the final manuscript.

Author's information
Chonghao Zhao (Student Member, IEEE) received the B.S. degrees in Electronic and Information Engineering from the Sichuan University (SCU), Chengdu, China, in 2021 and he is now pursuing a M.S. degree in information and communication engineering in the National Key Laboratory of Science and Technology on Communications (NCL), Chengdu, China. His research interests include optimization and learning in 5G/6G and signal processing in integrated sensing and communications (ISAC).
Gang Wu (Member, IEEE) received the B.E. and M.E. degrees from the Chongqing University of Posts and Telecommunications, Chongqing, China, in 1996 and 1999, respectively, and the Ph.D. degree from the University of Electronic Science and Technology of China (UESTC), Chengdu, China, in 2004. In June 2004, he joined UESTC, where he is currently a Professor with the National Key Laboratory of Science and Technology on Communications. He was a Research Fellow of the Positioning and Wireless Technology Centre, Nanyang Technological University, Singapore, from November 2005 to February 2007. He was a Visiting Professor with the Georgia Institute of Technology, Atlanta, GA, USA, from October 2009 to September 2010. His research interests include signal processing and resource management for 5G/6G and artificial intelligence for PHY/MAC design in wireless communications systems. He was a co-recipient of the IEEE GLOBECOM 2012 Best Paper Award. He is currently an Associate Editor of Science China Information Sciences, the Chair of IEEE Comsoc Chengdu Chapter, and the Secretary of the IEEE Chengdu Section.

Declarations

Ethics approval and consent to participate
Not applicable.

Consent for publication
Yes.

Competing interests
The authors declare that they have no competing interests.

References

1. L. Zhao, K. Yang, Z. Tan, X. Li, S. Sharma, Z. Liu, A novel cost optimization strategy for SDN-enabled UAV-assisted vehicular computation offloading. IEEE Trans. Intell. Transp. Syst. **22**(6), 3664–3674 (2020)
2. L. Zhao, K. Yang, Z. Tan, H. Song, A. Al-Dubai, A.Y. Zomaya, X. Li, Vehicular computation offloading for industrial mobile edge computing. IEEE Trans. Industr. Inf. **17**(11), 7871–7881 (2021)
3. 3GPP: Evolved universal terrestrial radio access (E-UTRA) and evolved universal terrestrial radio access network (E-UTRAN); overall description; stage 2. Technical Specification (TS) 36.300, 3rd Generation Partnership Project (3GPP) (December 2016). Version 14.1.0. https://portal.3gpp.org/desktopmodules/Specifications/SpecificationDetails.aspx?specificationId=2430
4. M. Amadeo, C. Campolo, A. Molinaro, Enhancing IEEE 802.11 p/wave to provide infotainment applications in VANETs. Ad Hoc Netw. **10**(2), 253–269 (2012)
5. 3GPP: Study on NR sidelink relay. Technical Report (TR) 38.836, 3rd Generation Partnership Project (3GPP) (March 2021). Version 17.0.0. https://portal.3gpp.org/desktopmodules/Specifications/SpecificationDetails.aspx?specificationId=3725
6. I. Ullah, Performance analysis of resource allocation and interference mitigation methods for inband decode and forward relaying. Ph.D. dissertation, Aalto University School of Electrical Engineering (June 2018)
7. 3GPP: Evolved Universal Terrestrial Radio Access (E-UTRA); Physical layer procedures. Technical Specification (TS) 36.213, 3rd Generation Partnership Project (3GPP) (September 2022). Version 15.16.0. https://portal.3gpp.org/desktopmodules/Specifications/SpecificationDetails.aspx?specificationId=2427
8. 3GPP: Study on NR-based access to unlicensed spectrum. Technical Report (TR) 38.889, 3rd Generation Partnership Project (3GPP) (December 2018). Version 16.0.0. https://portal.3gpp.org/desktopmodules/Specifications/SpecificationDetails.aspx?specificationId=3235
9. D. Wang, R.R. Sattiraju, A. Qiu, S. Partani, H.D. Schotten, Methodologies of link-level simulator and system-level simulator for C-V2X communication. In: 2019 IEEE 2nd International Conference on Electronics and Communication Engineering (ICECE), pp. 178–184 (2019). IEEE
10. R. Sattiraju, D. Wang, A. Weinand, H.D. Schotten, Link level performance comparison of C-V2X and ITS-G5 for vehicular channel models. In: 2020 IEEE 91st Vehicular Technology Conference (VTC2020-Spring) (IEEE, 2020), pp. 1–7
11. W. Anwar, S. Dev, A. Kumar, N. Franchi, G. Fettweis, PHY abstraction techniques for V2X enabling technologies: modeling and analysis. IEEE Trans. Veh. Technol. **70**(2), 1501–1517 (2021)
12. M. Schellmann, T. Soni, Ultra-reliable V2X communication: on the value of user cooperation in the sidelink. In: 2019 European Conference on Networks and Communications (EuCNC) (IEEE, 2019), pp. 570–574
13. B.R. Elbal, S. Schwarz, M. Rupp, Relay selection and coverage analysis of relay assisted V2I links in microcellular urban networks. In: 2020 IEEE Wireless Communications and Networking Conference (WCNC) (IEEE, 2020), pp. 1–7
14. Y. Hu, M.C. Gursoy, A. Schmeink, Relaying-enabled ultra-reliable low-latency communications in 5G. IEEE Netw. **32**(2), 62–68 (2018)
15. M. Noor-A-Rahim, G.M.N. Ali, Y.L. Guan, B. Ayalew, P.H.J. Chong, D. Pesch, Broadcast performance analysis and improvements of the LTE-V2V autonomous mode at road intersection. IEEE Trans. Veh. Technol. **68**(10), 9359–9369 (2019)
16. J. Fu, G. Wu, R. Li, Performance analysis of sidelink relay in SCMA-based multicasting for platooning in V2X. In: 2020 IEEE International Conference on Communications Workshops (ICC Workshops) (IEEE, 2020), pp. 1–6
17. G. Naik, J.-M.J. Park, Impact of Wi-Fi transmissions on C-V2X performance. In: 2019 IEEE International Symposium on Dynamic Spectrum Access Networks (DySPAN), pp. 1–10 (2019). IEEE
18. S.-Y. Lien, H.-L. Tsai, 3GPP V2X on unlicensed spectrum: performance analysis and optimum channel access strategies. IEEE Trans. Veh. Technol. **70**(9), 9230–9243 (2021)
19. T.J. O'Shea, J. Corgan, T.C. Clancy, Convolutional radio modulation recognition networks. In: Engineering Applications of Neural Networks: 17th International Conference, EANN 2016, Aberdeen, UK, September 2–5, 2016, Proceedings 17, pp. 213–226 (2016). Springer

20. S. Rajendran, W. Meert, D. Giustiniano, V. Lenders, S. Pollin, Deep learning models for wireless signal classification with distributed low-cost spectrum sensors. IEEE Trans. Cogn. Commun. Netw. **4**(3), 433–445 (2018)
21. Z. Zhang, H. Luo, C. Wang, C. Gan, Y. Xiang, Automatic modulation classification using CNN-LSTM based dual-stream structure. IEEE Trans. Veh. Technol. **69**(11), 13521–13531 (2020)
22. M. Schmidt, D. Block, U. Meier, Wireless interference identification with convolutional neural networks. In: 2017 IEEE 15th International Conference on Industrial Informatics (INDIN), pp. 180–185 (2017). IEEE
23. G. Liu, Z. Xi, R. Liu, A novel wireless interference identification and scheduling method based on convolutional neural network. In: 2022 IEEE International Conference on Communications Workshops (ICC Workshops), pp. 1–6 (2022). IEEE
24. 3GPP: NR; Physical channels and modulation. Technical Specification (TS) 38.211, 3rd Generation Partnership Project (3GPP) (June 2022). Version 16.10.0. https://portal.3gpp.org/desktopmodules/Specifications/SpecificationDetails.aspx?specificationId=3213
25. 3GPP: NR; Multiplexing and channel coding. Technical Specification (TS) 38.212, 3rd Generation Partnership Project (3GPP) (June 2022). Version 16.10.0. https://portal.3gpp.org/desktopmodules/Specifications/SpecificationDetails.aspx?specificationId=3214
26. 3GPP: NR; Physical layer procedures for data. Technical Specification (TS) 38.214, 3rd Generation Partnership Project (3GPP) (September 2022). Version 16.11.0. https://portal.3gpp.org/desktopmodules/Specifications/SpecificationDetails.aspx?specificationId=3216
27. 3GPP: Study on evaluation methodology of new Vehicle-to-Everything (V2X) use cases for LTE and NR. Technical Report (TR) 38.885, 3rd Generation Partnership Project (3GPP) (June 2019). Version 15.3.0. https://portal.3gpp.org/desktopmodules/Specifications/SpecificationDetails.aspx?specificationId=3209
28. M. Kahn, IEEE 802.11 regulatory SC DSRC coexistence tiger team V2V radio channel models. IEEE 802.11-14/0259r0 **28** (2014)
29. IEEE: 11ax Evaluation Methodology. Document 802.11-14/0571, Institute of Electrical and Electronics Engineers (IEEE) (January 2016). Version r12. https://mentor.ieee.org/802.11/dcn/14/11-14-0571-12-00ax-evaluation-methodology.docx
30. S. Bai, J.Z. Kolter, V. Koltun, An empirical evaluation of generic convolutional and recurrent networks for sequence modeling. arXiv preprint arXiv:1803.01271 (2018)
31. M. Chen, U. Challita, W. Saad, C. Yin, M. Debbah, Artificial neural networks-based machine learning for wireless networks: a tutorial. IEEE Commun. Surv. Tutor. **21**(4), 3039–3071 (2019)
32. 3GPP: NR; User Equipment (UE) radio transmission and reception; Part 1: Range 1 Standalone. Technical Specification (TS) 38.101-1, 3rd Generation Partnership Project (3GPP) (September 2022). Version 16.13.0. https://portal.3gpp.org/desktopmodules/Specifications/SpecificationDetails.aspx?specificationId=3283
33. H. Zhou, T. Wu, H. Zhang, J. Wu, Incentive-driven deep reinforcement learning for content caching and D2D offloading. IEEE J. Sel. Areas Commun. **39**(8), 2445–2460 (2021)
34. H. Zhang, M. Huang, H. Zhou, X. Wang, N. Wang, K. Long, Capacity maximization in RIS-UAV networks: a DDQN-based trajectory and phase shift optimization approach. IEEE Trans. Wirel. Commun. (2022)
35. 3GPP: Evolved Universal Terrestrial Radio Access (E-UTRA); Base Station (BS) radio transmission and reception. Technical Specification (TS) 36.104, 3rd Generation Partnership Project (3GPP) (April 2022). Version 16.13.0. https://portal.3gpp.org/desktopmodules/Specifications/SpecificationDetails.aspx?specificationId=2412

Publisher's Note